Microstructure and Dynamic Mechanical Behavior of Thermomechanically Rolled 3Mn–Al and 5Mn–Al Sheet Steels

Morawiec, Mateusz; Grajcar, Adam; Krawczyk, Jakub; Gronostajski, Zbigniew; Petrov, Roumen H.

Important note
To cite this publication, please use the final published version (if applicable).
Please check the document version above.

Microstructure and Dynamic Mechanical Behavior of Thermomechanically Rolled 3Mn–Al and 5Mn–Al Sheet Steels

Mateusz Morawiec, Adam Grajcar,* Jakub Krawczyk, Zbigniew Gronostajski, and Roumen H. Petrov

The comparison of the dynamic mechanical behavior and microstructure of two medium manganese sheet steels (3Mn–Al and 5Mn–Al) alloyed with aluminum is aimed. Mechanical properties under dynamic tensile loads are determined by means of rotary hammer dynamic tests at strain rates of 250 and 1000 s^{-1} and analyzed together with the results of static tensile test. It is found that the results are significantly affected by the variations in Mn content in the range from 3 to 5 wt%. In both steels, the tensile strength increases with increasing strain rate, but the variation in the strain rate range has a moderate effect on mechanical behavior. The highest ultimate tensile strength of 1475 MPa is measured in the 5Mn–Al steel, whereas the 3Mn–Al steel is characterized by better total elongation due to a larger fraction of retained austenite and more pronounced transformation-induced plasticity effect. The results show that the mechanical properties of 3Mn steel are more strain rate sensitive than those of 5Mn steel. The microstructural features are characterized qualitatively and quantitatively by X-ray diffraction, scanning electron microscopy, and electron back-scattered diffraction techniques.

1. Introduction

Nowadays, the automotive industry is undergoing intensive development due to the need to implement electromobility in public transport. This is related to the need to reduce the negative impact on the environment, and at the same time to switch to other types of fuel, as oil reserves drastically decrease and the demand for fuels increases.[1,2] The use of electrical systems in passenger cars causes an increase in their mass due to the weight of energy storage batteries. At the same time, the increase in the mass reduces maximum loads that can be travelled. Moreover, the increase in weight negatively affects the passive safety of passenger cars, and the optimization of the battery position is necessary.[3] Therefore, it is important to use high-strength materials that allow to maintain high safety, while reducing the maximum weight of the vehicle.

The ferrous alloys currently used in the automotive industry belong to the 1st generation of advanced high-strength steels (AHSS).[4] These steels are characterized by multiphase structure composed of various phases, such as ferrite, martensite, retained austenite (RA), and/or microstructural constituents like bainite. The most common type of first-generation AHSS are dual-phase steels composed of ferrite and martensite and TRIP-aided (transformation-induced plasticity) multiphase steels. TRIP-aided AHSS are characterized by the presence of RA in the microstructure, which undergoes strain-induced martensitic transformation (SIMT) during technological metal forming, increasing the mechanical properties of the steel.[5] In industrial practice, this transformation allows for the production of elements of complex shape. Such design allows for the absorption of more energy during collision events and at the same time its further distribution to other elements of the vehicle responsible for safety.[6,7] Among the newest groups of advanced multiphase steels are the medium-manganese steels with a manganese content ranging from 3% to 12%,[8] which belong to the third generation of AHSS. The increased content of manganese in these steels is responsible for increasing the proportion of RA in the microstructure, which allows for improved mechanical properties.[9,10]

M. Morawiec
Materials Research Laboratory
Silesian University of Technology
18a Konarskiego Street, 44-100 Gliwice, Poland

A. Grajcar
Department of Engineering Materials and Biomaterials
Silesian University of Technology
18a Konarskiego Street, 44-100 Gliwice, Poland
E-mail: adam.grajcar@polsl.pl

J. Krawczyk, Z. Gronostajski
Department of Metal Forming, Welding and Metrology
Wroclaw University of Science and Technology
7-9 Łukasiewicza Street, 50-371 Wrocław, Poland

R. H. Petrov
Department of Electromechanical, Systems and Metal Engineering
Ghent University
Tech Lane Ghent Science park-Campus A Zwijnaarde, Technologiepark 46, 9052 Ghent, Belgium

R. H. Petrov
Department of Materials Science and Engineering
Delft University of Technology
3mE-TUDelft
Building 34, Mekelweg 2, 2628 CD Delft, The Netherlands

In case of forming structural elements of the car body, methods such as stamping, bending, hydroforming, characterized by a high strain rate, are used.[11] Under the conditions of dynamic technological forming, the materials show different properties than in case of static conditions, what is the result of higher strain levels and the change in a material temperature. Gronostajski et al.[12] found that during the dynamic deformation of AHSS sheets, the global temperature of the material may increase by 100 °C, and even reach 500 °C near the necking area of a sample. This is very important as temperature has a great influence on the stability of the RA. Kozłowska et al.[13] reported that austenite stability increases when the deformation temperature is ≥ 100 °C. It is related to an increase in the stacking fault energy (SFE) of austenite with increasing temperature. The change of RA stability has high impact on mechanical properties of steel. According to Poling et al.,[14] the increase of temperature during deformation results in the decrease of work hardening rate, ultimate tensile strength, and elongation, leading to lower mechanical properties of medium-Mn steels. This is the result of high RA stability that results in small dynamic SIMT effect. The similar result was reported by Sevsek et al.[15] in intercritically annealed 0.064C–12Mn–2.8Al steel subjected to low and high strain rates. They showed that the increase of strain rate deteriorates the mechanical properties at the low (<0.001 s^{-1}) and medium ($0.001 \div 1$ s^{-1}) strain rates. With increasing the strain rate above 1 s^{-1}, the increase of total elongation and ultimate tensile strength took place. He et al.[16] noted that the strain rate affected the elongation of 3.5% and 10% medium-Mn steels. They reported that the elongation values decreased in both steels at strain rates up to 450 s^{-1}. However, when the strain rate was near 1200 s^{-1}, the elongation of both steels increased. The above-described effects are the result of change in the RA stability stimulated by temperature changes.

Another aspect is a deformation type. Kim et al.[17] reported that the SIMT occurs most easily during stretching and less intense during compression. Another interesting phenomenon was observed by Wang and Huang,[18] which analyzed the influence of strain rate on mechanical properties of 3Mn steel. Under static conditions, serrations were registered on tensile curves due to the occurrence of dynamic strain aging (DSA). However, when they increased the strain rate to 1000 s^{-1}, this effect disappeared. The reason was the very fast movement of dislocations, which made it impossible for them to be anchored by interstitial atoms.

The above-described issues indicate the need to analyze the behavior of steel under the conditions of dynamic deformation, especially in case of newly developed thermomechanically processed multiphase steels. The current study will allow for the systematization of knowledge in the field of the impact of dynamic deformation on microstructure–dynamic mechanical property relationships of hot-rolled multiphase steels. It is important because in case of crush events, the metal behavior is critical for the safety of the passengers. Static tests give only approximation of the mechanical parameters, but the real data can be obtained by dynamic tests. Moreover, the high strain rate deformation behavior of metals gives opportunities to implement high strain rate metal-forming technologies, where the productivity can increase significantly. So far, works in the field of high strain rate for medium manganese steels refer to cold rolled and intercritically annealed steels. Less attention is paid to

thermomechanically rolled steels. Such research may extend the existing knowledge in the field. Therefore, this work analyzes the influence of the strain rate on the mechanical properties and microstructure of two medium-Mn steels containing 3% and 5% manganese.

2. Experimental Section

2.1. Material

The chemical composition was determined using glow discharged optical emission spectroscopy (GDOES). Three analyses were carried out, and the mean values are presented in **Table 1**. The steels contain aluminum and silicon additions to prevent the carbide precipitation during the bainite transformation[13] and to stabilize the RA in the final microstructure. There is only the difference in an Mn content between both melts, whereas the rest of alloying elements is at the same level. Therefore, we denoted the steels as 3Mn and 5Mn regarding to the manganese addition.

The 0.2% of Mo was added to increase hardenability and prevent the manganese embrittlement during hot-working processes (forging and hot rolling). This effect can be present in the steels containing above 3% Mn.[19] The manganese atoms tend to segregate into prior austenite grain boundaries resulting in the embrittlement of steel. The addition of Mo prevents this harmful effect.[20]

Both steels were melted using a laboratory VSG-50 vacuum induction furnace by Balzers in an argon atmosphere. Then, the ingots were hot forged using a high-speed hydraulic press to obtain flat bars with a cross section of 22×170 mm. Forging was carried out in the temperature range of 1200–900 °C. Before rough rolling, the steel bars were homogenized at 1200 °C for 3 h and after that the 22 mm thick bars were rolled in 4 passes to a thickness of 9 mm. Finally, the as produced plates with dimensions of $9 \times 170 \times 500$ mm were subjected to thermomechanical rolling using the semi-industrial hot rolling line.[21] The thermomechanical treatment involved rolling the 9 mm plates in three passes to a final thickness of 4.5 mm. The finishing rolling temperature for both steels was 850 °C (**Figure 1**), which is below the A_{r3} temperature of the steels. The only difference in a cooling profile was that after the following rolling 3Mn steel was air cooled for 10 s to eventually produce some ferrite fraction in the microstructure. Next, both steels were cooled to 400 °C at the rate of 27 °C s^{-1}, at which they were isothermally held in the in-line furnace within 300 s to produce bainite and stabilize some austenite amount.

Manganese, as the austenite stabilizer, should increase the maximum amount of RA after heat treatment. The microstructure of the 3Mn steel was composed of bainitic ferrite (BF), RA, and martensitic-austenitic islands. The 10 s cooling following rolling does not induce any ferrite in the microstructure. In case

Table 1. Chemical compositions of analyzed steels.

Steel	C [wt%]	Mn [wt%]	Al [wt%]	Si [wt%]	Mo [wt%]
3Mn	0.17	3.3	1.7	0.22	0.23
5Mn	0.16	4.7	1.6	0.20	0.20

**ADVANCED
SCIENCE NEWS**

www.advancedsciencenews.com

steel
research
international
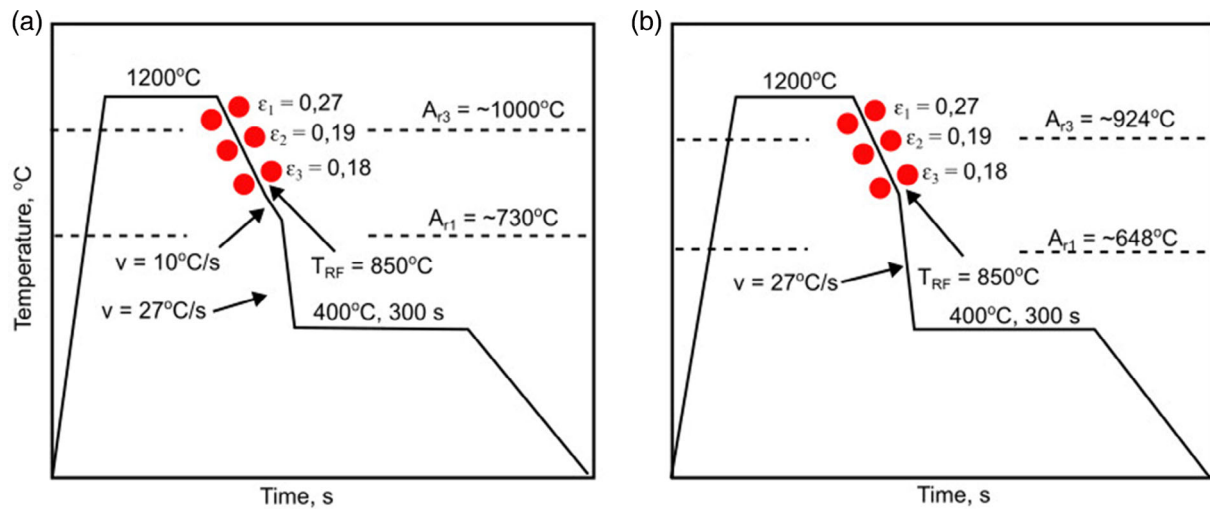
www.steel-research.de

Figure 1. The thermomechanical rolling of: a) 3Mn, b) 5Mn steels.

of higher hardenability 5Mn steel, the microstructure is composed of bainite, the high amount of martensite occurring as martensitic-austenitic (MA) islands, and some fraction of RA. Some intralath carbide precipitates are present in the steel of the higher Mn addition. Both initial microstructures are presented in **Figure 2**ab.

To identify the steels deformed at the particular strain rate the following denotation has been applied: $3Mn\_250\,s^{-1}$ (as an example for 3Mn steel), for example, as a deformation variant corresponding to the 3Mn steel deformed at the strain rate of $250\,s^{-1}$. In the same way, the deformed 5Mn steel was denoted.

2.2. Dynamic Tensile Tests

Dynamic tensile tests were performed using a rotary impact hammer-type RSO manufactured by WPM Lipsk. The rotary hammer allows for deformation of samples with a linear speed of the handle displacement in the range of 3.5–$50\,m\,s^{-1}$, which corresponds to the strain rate in the range of $10^2 \div 3 \times 10^3\,s^{-1}$ depending on the length of the sample base. A sample was attached to the upper handle of the measuring 6 m long rod

and to the lower handle. Dynamic stretching of the sample was performed using the hammer, which hits the lower anvil causing its deformation. The hammer rotating in the hammer disc, locked in the socket, was released electromagnetically at a certain rotational speed. The tilted hammer hits the lower holder causing the sample to break. The high kinetic energy of the rotating disc compared to the strain energy of the sample ensures a constant tensile rate during the test.[12]

The 6 mm width and 14 mm gauge length samples were prepared for each of the analyzed steels (the total length and width of the dog bone samples were 64 and 20 mm, respectively, according to **Figure 3**). For each variant, three samples were tested, and the curve closed to the average was presented in the manuscript.

In order to simulate deformation conditions similar to the ones during crush events, strain rates of 250 and $1000\,s^{-1}$ were applied.

2.3. Microstructure Investigation

The samples for metallographic investigations were prepared by conventional sample preparation procedures. The material after
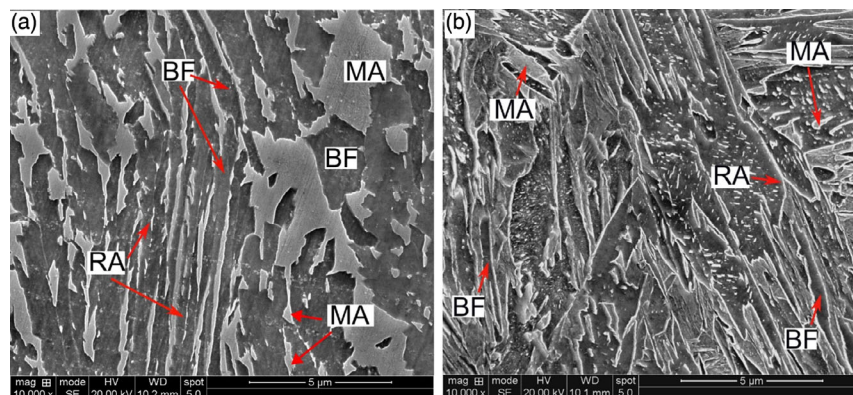

Figure 2. Initial microstructures of both analyzed steels: a) 3Mn, b) 5Mn; BF—bainitic ferrite, MA—martensitic-austenitic islands, RA—retained austenite.
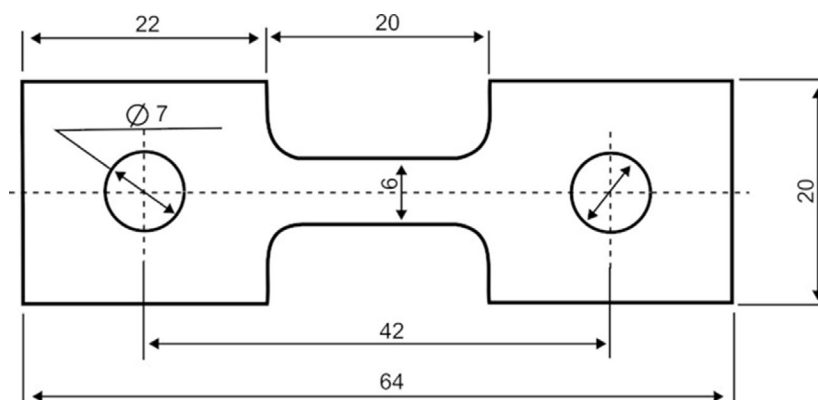
2200908 (3 of 10)

ADVANCED
SCIENCE NEWS
www.advancedsciencenews.com

steel
research
international

www.steel-research.de

Figure 3. The dog bone sample used for the dynamic tests.

the dynamic deformation was cut from the sample in some distance ($\approx$ 2 mm) from the fracture area. The materials were grinded using papers from 220 up to 2000. After grinding the material was polished using diamond solutions of 3 and 1 μm and etched in 3% Nital to reveal microstructural constituents. The microstructure investigation was carried out using FEI Quanta FEG 450 scanning electron microscope. For the electron backscatter diffraction (EBSD) analysis, the samples were additionally polished using colloidal silica for 40 min to obtain good indexation during the mapping. The EBSD was conducted using OIM TSL data collection software v. 7.3. The sample tilt of 70°, a working distance of 15 mm and accelerating voltage of 20 kV were used. The scans were performed on an area of 10×10 μm^2 with a step size of 0.03 μm and a hexagonal scan grid. The samples used for the X-ray diffraction (XRD) analysis to determine the RA amount were polished and etched few times to remove the deformed layer, where the RA could be transformed into martensite during grinding. For the XRD, the cobalt anode ($\lambda K_\alpha = 0.179$ nm) and the PIXcel 3D-detector on the diffracted beam axis were used. The diffraction lines were recorded in the Bragg–Brentano geometry in the angular range of 45°–105° with a step of 0.026° and a scan speed of 0.6 s step^{-1}. The analysis of the registered diffraction patterns was carried out using High Score Plus software v. 3.0 containing a dedicated inorganic crystal structure database (PAN-ICSD). The thermodynamic calculations of the SFE were carried out using JMatPro software using the general steel module, database ver. 13.[22]

3. Results

3.1. Dynamic Tensile Tests

Figure 4 presents the dynamic tensile curves for both steels at two different strain rates. The yield point cannot be determined because the curves are distorted as a result of high moment of inertia in the initial dynamic deformation stage (especially for the samples deformed at 1000 s^{-1}). It is present due to the hammer strike to the anvil, where samples are fixed. It can be seen that the 3Mn steel exhibits lower strength and higher plasticity compared to the 5Mn steel. The reason is the high amount of hard martensite constituents in 5Mn steel.
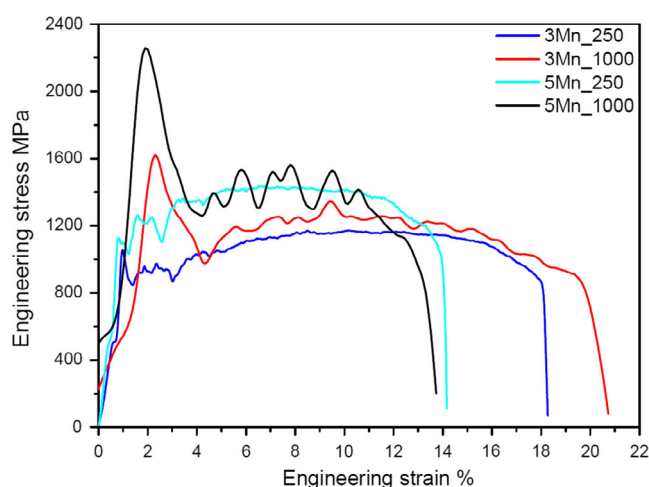

Figure 4. The dynamic tensile curves for analyzed steels registered at two strain rates.

Martensite as a hard phase increases the maximum strength, however, at the expense of lower ductility. The bainitic matrix, which is present in the 3Mn steel, lowers its strength but provides some higher plasticity. It is visible that increasing the strain rate from 250 to 1000 s^{-1} does not affect significantly the tensile strength of steels. Some influence on the plasticity can be seen, yet the trend is little different for the 3Mn and 5Mn steels. **Table 2** presents the comparison of tensile strength and total elongation between static and dynamic tensile tests. As can be

Table 2. Mechanical properties registered under static and dynamic conditions for both steels.

Steel	Static		Dynamic		Strain rate [s^{-1}]
	Rm [MPa]	TEl [%]	Rm [MPa]	TEl [%]	
3Mn	957	15	1181	18	250
			1255	21	1000
5Mn	1215	12	1475	14	250
			1480	13	1000

seen, the tensile strength is higher, when dynamic loads are applied. For 3Mn and 5Mn steels, the tensile strength increases by 300 and 250 MPa, respectively. The authors in work[23] explained that a rise in the strength during dynamic deformation depends on an initial strength level of the material registered under static conditions. During the dynamic deformation, the steel exhibiting a lower tensile strength during static tests shows a higher strength increase potential compared to the high-strength steels composed of hard phases only. This explains why the 3Mn steel is strengthened to the higher extent. The similar trend is present in case of total elongation, where it was noticed that under dynamic conditions the steels show higher levels of ductility. However, this is more complicated aspect of the dynamic deformation, as it is additionally influenced by the TRIP effect, a sample geometry,[12] and a temperature rise of the sample,[13] especially in the necking area.

3.2. Microstructure Results

The microstructures after dynamic deformation are presented in **Figure 5**. One can see a high number of MA islands due to the dynamic strain-induced austenite to martensite transformation in both steels. Therefore, the 3Mn steel contains now bainitic microstructure as a matrix and some amount of martensitic-austenitic islands, whereas the 5Mn steel is composed of initial and strain-induced MA islands and some bainite fraction. The higher bainitic fraction in the 3Mn steel enhances its plasticity compared to the 5Mn steel. However, at the same time, it

decreases the maximum strength. In both steels, the strain rate in a range from 250 to $1000 \, s^{-1}$ does not have a significant influence on the microstructure of the steels. Moreover, no adiabatic shear bands (ASB) were present in the microstructure of the steels. This is due to relatively low strength levels of the steels. According to refs. [24,25], the formation of ASB is common during dynamic deformation. However, this is true only for steels with ultrahigh strength levels like nano-bainitic steels or martensitic steels (the steels with a strength level of 2000 MPa).

Figure 6 presents the kernel average misorientation (KAM) maps together with low- and high-angle grain boundaries. When analyzing their fractions, it can be noticed that in case of both steels, these fractions are different. 3Mn steel, deformed at a rate of $250 \, s^{-1}$, contains mainly high-angle grain boundaries (HAGB) and strain concentration (SC) regions (Figure 6a). However, when the strain rate is increased to $1000 \, s^{-1}$, the proportion of low-angle boundaries (LAGB) increases significantly at the expense of strain concentration. This can be seen in Figure 6b, where the map shows fine grains with low-angle grain boundaries (white lines). In case of 5Mn steel, it can be seen that at $250 \, s^{-1}$ (Figure 6c), there are more low-angle grain boundaries in the microstructure than in the 3Mn steel deformed at the same rate. However, the fine grains in the structure are characterized by high-angle grain boundaries. When the strain rate was increased to $1000 \, s^{-1}$, high-angle grain boundaries dominated the structure as presented in Figure 6d.

In order to determine the potential presence of RA in the steel microstructure after plastic deformation, phase distribution and
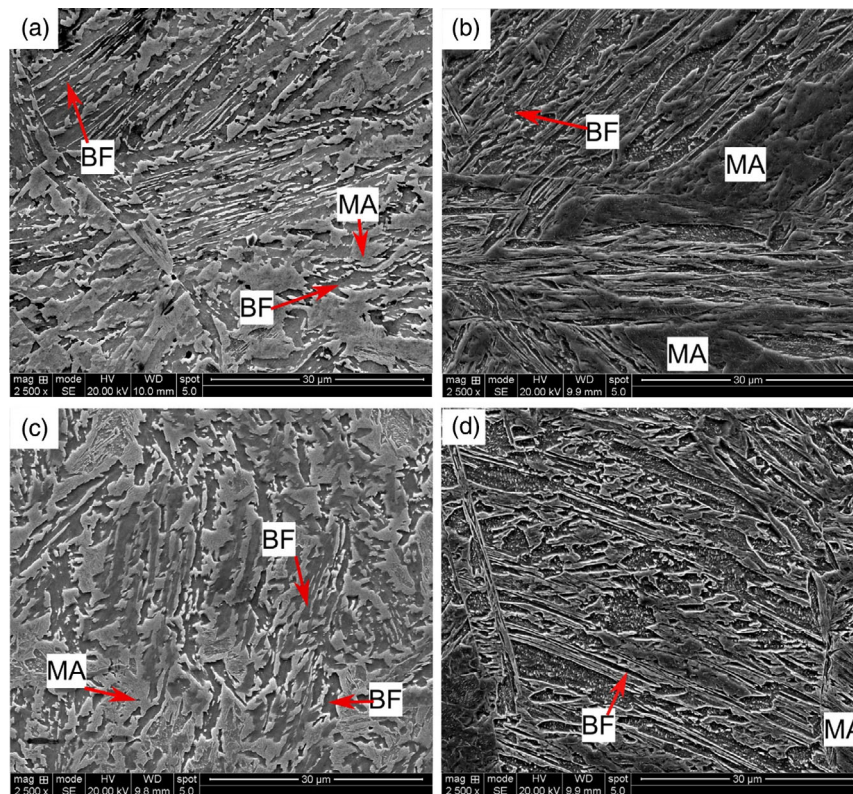

Figure 5. The microstructures of the 3Mn and 5Mn steels after dynamic deformation: a) 3Mn_250, b) 5Mn_250, c) 3Mn_1000, and d) 5Mn_1000; BF—bainitic ferrite, MA—martensitic-austenitic islands.
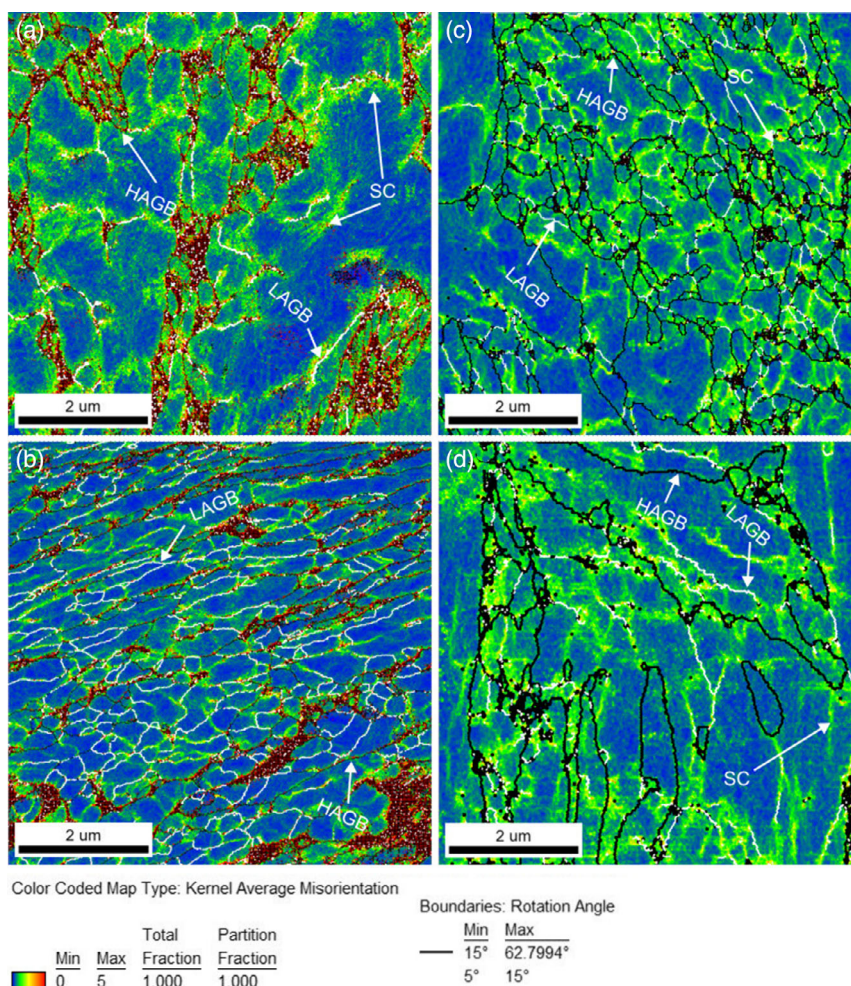
ADVANCED
SCIENCE NEWS

www.advancedsciencenews.com

steel
research
international

www.steel-research.de

Figure 6. The KAM and grain boundaries distribution maps for: a) 3Mn-250s^{-1}, b) 3Mn-1000s^{-1}, c) 5Mn-250s^{-1}, and d) 5Mn-1000s^{-1} steels; SC—strain concentration, LAGB—low-angle grain boundaries, HAGB—high-angle grain boundaries.

image quality maps were analyzed in more detail. According to the phase maps shown in **Figure 7**, it can be seen that no RA was found in both steels. This means that most of RA has been transformed during plastic deformation into martensite. However, it should be also taken into account that potential austenite at grain boundaries might be not indexed even when it is not
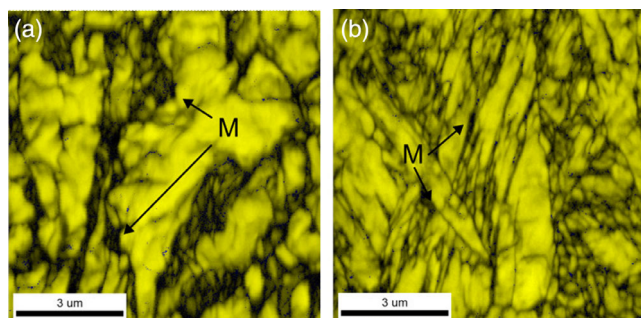
transformed to martensite. Hence, some little amount of this phase may be present as MA islands. This can be seen as the black areas on the maps, corresponding to low indexation of the structure (highly deformed).

Additionally, in the image quality (IQ) maps (**Figure 8**), the areas with the lowest image quality were highlighted in light blue. For this purpose, the grain average image quality charts were used (Figure 8c,d) to select a range of IQ values highlighted in the IQ maps. These areas represent the strain-induced martensite characterized by high dislocation density.[26] For the 3Mn steel, the amount of the highlighted areas is higher as this steel contains the higher RA fraction before being deformed. As the 5Mn steel has higher hardenability, the amount of RA in the initial state is smaller. Hence, the lower amount of highly dislocated martensite can be expected. According to these analyses, the amount of highly deformed martensite is ≈14% and 7% for 3Mn and 5Mn steels, respectively. These values are close to the initial amounts of RA, which means that almost all austenite transformed into martensite during dynamic deformation.

Since the EBSD technique is the surface-type analysis, the XRD analysis was also carried out to determine RA amount in
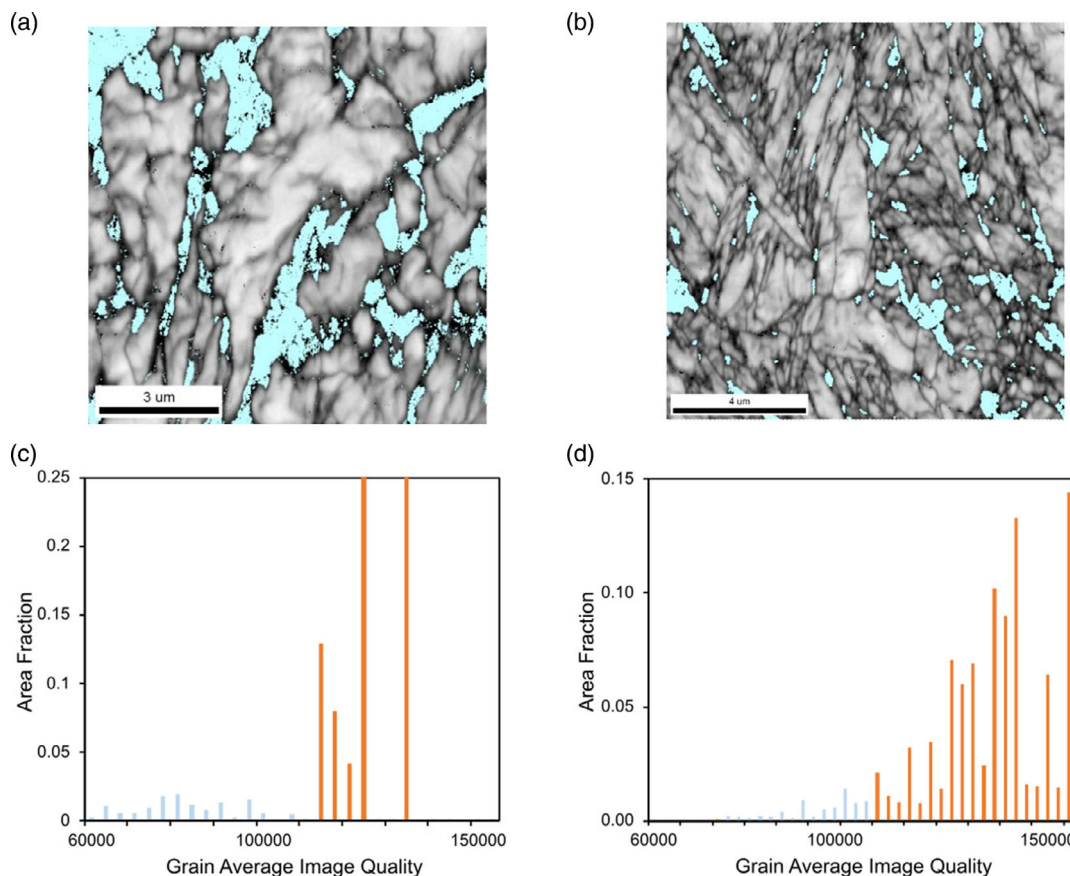

Figure 7. The IQ and phase maps for: a) 3Mn-250s^{-1}, b) 5Mn-250s^{-1} steels: yellow regions represent alpha phases, and blue regions correspond to the remaining traces of the gamma phase; M—martensite.

Figure 8. The IQ maps for: a) 3Mn-250s^{-1}, b) 5Mn-250s^{-1} steels, c–d) the grain average image quality charts for 3Mn (c) and 5Mn (d) steels used to highlight the strain-induced martensite showing the lowest IQ values.

the samples. According to the XRD results listed in **Table 3**, no RA was also present in the microstructure after dynamic deformation (or <2%, which is an accuracy of the XRD method). It means that under such dynamic conditions all the austenite transformed into martensite during deformation increasing the mechanical properties of the steels, which is in line with the EBSD results.

4. Discussion

4.1. Stress and Strain Behavior during Dynamic Deformation

On the basis of the presented results, it can be seen that mechanical properties of both steels are significantly higher compared to static conditions. As presented in **Figure 9**, the tensile strength of

Table 3. XRD results of retained austenite fractions in steels.

Steel	RA in initial state [%]	Strain rate [s^{-1}]	RA [%]
3Mn	13 ± 2	250	<2
		1000	<2
5Mn	10 ± 2	250	<2
		1000	<2

the 3Mn steel increases by 224 and 298 MPa at 250 and 1000 s^{-1} strain rates, respectively. In case of 5Mn steel, the strength increases by 260 and 265 MPa, respectively.

The higher strength properties of dynamically deformed alloys are confirmed by many authors[15,27] not only for steels.[28,29] According to Wang et al.,[30] this increase may be caused by two factors: slower dislocation annihilation and an increase in
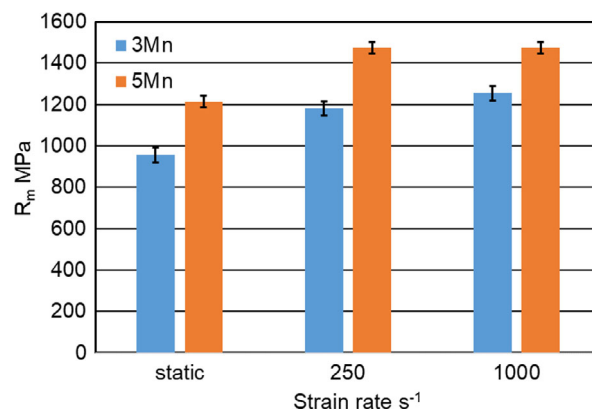

Figure 9. The change of tensile strength for both steels during static and dynamic tensile tests.

the number of obstacles to dislocation movement. Fan et al.[29] investigated the effect of dislocation density and strain rate on mechanical properties of copper and aluminum alloys. They reported that the strength depends on the presence of two strengthening factors. The first one assumes that the yield point increases proportionally to the strain rate and inversely proportional to the dislocation density at the yield point. The second factor is related to forest dislocations. In this mechanism, the yield point is independent of the strain rate and corresponds to the Taylor dependence. Alabi et al.[27] analyzed a change in mechanical properties of three different steels (S235, S690QL, and S960QL) under strain rate conditions up to $100 \, s^{-1}$. According to their results, the lower the yield point, the greater increase in strength under dynamic conditions is achieved. In the case of S235 steel with the lowest yield point, this increase was 66%. However, in the case of S690QL and S960QL steels of higher yield strength levels, it was, respectively, only 9% and 6%. These results show that changes in the strength properties under dynamic deformation conditions strongly depend on the stress state in the material before deformation, resulting from the dislocation density or a type of structural constituents. This corresponds to the results obtained in the current study, when comparing the mechanical properties of 3Mn and 5Mn steels deformed under static and dynamic conditions. The higher increase in strength ($\approx$24%) was recorded for the 3Mn steel, which is characterized by the lower initial yield point (smaller amount of hard phases compared to the 5Mn steel). For the 5Mn steel, the strength under dynamic conditions increased by 18% compared to static conditions.

In case of plastic properties, it can also be seen that the application of dynamic deformation caused an increase in the total elongation of both steels (**Figure 10**). However, this increase is more noticeable for the steel with a lower manganese content due to the presence of bainitic matrix with RA in the microstructure. The increase of total elongation values between static and dynamic deformation is $\approx$17% (at $250 \, s^{-1}$) and $\approx$30% (at $1000 \, s^{-1}$). The 5Mn steel shows a smaller elongation gain of 14%. At the same time, one can see that increasing the strain rate from 250 to $1000 \, s^{-1}$ increased the total elongation of 3Mn steel (by 14%), but a small decrease was registered for 5Mn steel ($\approx$5%). This is similar to the results reported by Gronostajski

et al.,[12] who reported a continuous increase in uniform and total elongation in a strain rate range from 0.5 to $1000 \, s^{-1}$ in DP600 and TRIP690 steels. Chiyatan and Uthaisangsuk,[31] in their work on the dynamic deformation of DP steels found that the uniform elongation of the DP1000 steel increases with a strain rate increase. Similarly, Van Slycken et al.[32] investigated two TRIP-aided multiphase steels containing aluminum and silicon (separately). They also observed a significant increase in elongation compared to the static conditions. In both cases, the total elongation increased twice compared to the static deformation. At the same time, they reported that the total elongation increased only slightly with increasing strain rate in a range from 1000 to $2000 \, s^{-1}$. This corresponds to the results presented in the current study, where the increase of total elongation is registered in the range between 250 and $1000 \, s^{-1}$.

Similar results were obtained by Rong et al.[33] who analyzed the influence of strain rate on TRIP-aided multiphase steel with a low silicon content, similar as in case of the analyzed steels. According to their results, an increase of strain rate causes a rise of total elongation. They reported that this is related to the temperature increase, which increases the stability of the RA. This causes that the TRIP effect is shifted to higher deformation levels and dominates the neck formation during the tensile test. The continuous transformation of austenite into martensite slows the formation of the neck in this range, which ultimately increases the total elongation. Similar results were reported for medium-Mn steels.[14–16] However, in their case, mechanical properties are more strain rate dependent.[16] Some works reported that the TRIP effect is delayed or limited due to the temperature increase caused by the increased strain rates[14,15] leading to a decrease of tensile strength. Poling et al.[14] stated that depending on the deformation temperature, the amount of the RA transformed can change as far as 38% (at 20 °C) to 10% (at 115 °C). The influence of temperature on the RA stability is the most often reported reason for the change in the plasticity of multiphase steels. According to ref. [34], even an increase of the strain rate from 0.001 to $0.5 \, s^{-1}$ results in the increase of the sample temperature from 40 up to 100 °C in the necking region. The change of RA stability can increase the necessary strain limit for the TRIP effect to occur or even stop the transformation resulting in a decrease of mechanical properties.
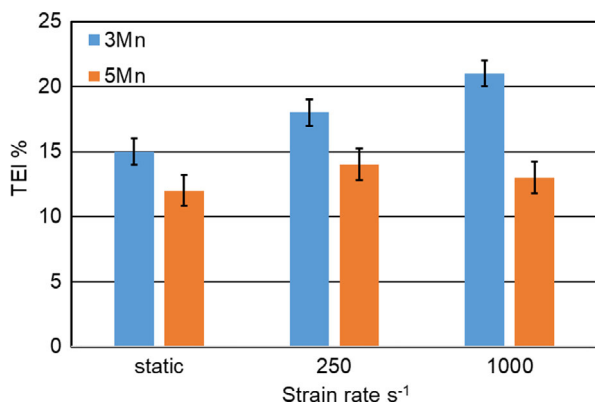
4.2. Microstructure after Dynamic Deformation

According to the XRD results, no RA was identified in the microstructure after dynamic deformation. The XRD results indicated that in both cases, its entire fraction was transformed into strain-induced martensite. The same result was obtained by the EBSD analysis of the image quality maps. The amount of highly deformed strain-induced martensite in the 3Mn steel was $\approx$14% and $\approx$7% in 5Mn steel. These values correspond to the amount of RA in the material before dynamic deformation. In contrast, some austenite after deformation could be expected due to a rise in temperature of the deformed sample.[13] The increase in temperature affects simultaneously a rise of the SFE and results in the increase of RA stability. The higher the temperature, the higher SFE of the RA. Talonen et al.[35] investigated the intensity of martensitic transformation in three

Figure 10. The change of total elongation for both steels during static and dynamic tensile tests.

different austenitic stainless steels deformed in a strain range from $3 \times 10\,s^{-4}$ to $200\,s^{-1}$. They reported that the adiabatic heating accompanying the tensile deformation at high strain levels inhibits the SIMT due to the reduction of the driving force of the austenite to martensite transformation. This effect is illustrated in **Figure 11**, which shows that the calculated (using JMatPro software) SFE of both investigated steels is very similar and rises in a similar way with increasing deformation temperature. In case of material temperature in the range of 100–200 °C, which is often reported in literature, it causes an increase of the SFE in the range of $20–50\,mJ\,m^{-2}$.

However, the closer to the neck, this temperature can reach even 500 °C.[12] Such a high temperature significantly increases further the SFE resulting in strong stabilization of the RA. Another effect indicating the presence of high temperature during dynamic deformation is a change in the amount of low- and high-angle grain boundaries shown in Figure 6. In case of 3Mn steel deformed at $250\,s^{-1}$, the high dislocation density is present (reflected in Figure 6a presenting the KAM map of 3Mn steel). However, when the strain rate increased to $1000\,s^{-1}$, the dislocation density decreased and a significant increase in the amount of fine grains characterized by low-angle boundaries was observed. This effect may indicate the occurrence of dynamic recovery,[36] which requires the formation of subgrains in the microstructure. At the same time, in 5Mn steel, some amount of fine grains with low-angle and high-angle grain boundaries can be already seen in the sample deformed at $250\,s^{-1}$. With increasing the strain rate to $1000\,s^{-1}$, the proportion of grains with low-angle boundaries significantly decreases. This suggests that in case of 5Mn steel of higher initial strength, plastic deformation must be accompanied by higher temperature rise than in 3Mn steel. This could explain the dominance of the low-angle substructure for the steel containing a lower manganese content. Moreover, this is in line with the lower work strengthening of the 5Mn steel (the higher temperature increase), which can be noted when comparing the tensile curves for both steels in Figure 4.

Although increased temperatures accompany the dynamic deformation, no RA was detected in the microstructure of both steels. This may be due to the way the material is deformed. The martensitic transformation of the RA is accompanied by a corresponding volume increase. This means that some adequate space must be provided for the newly formed martensite.
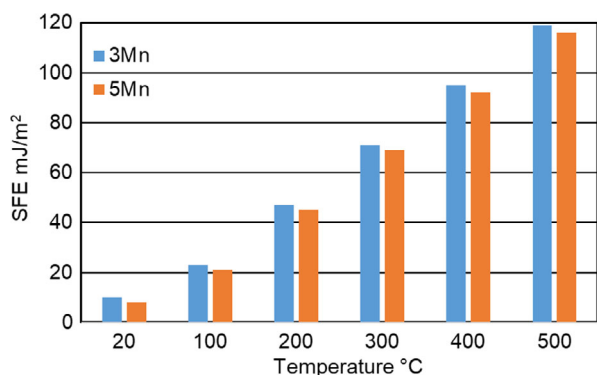

Figure 11. Stacking fault energy of both steels as a function of deformation temperature (JMatPro).

When the sample is tensile deformed, the microstructure also stretches with a continuous volume increase. This, in turn, facilitates the martensitic transformation of the RA as it has a free space to be formed.

Kim et al.[17] reported that RA transforms more easily when the sample is stretched than subjected to compression. In case of compression, the stresses acting on the RA act opposite compared to the tension. Hence, it is more difficult to form martensite during deformation because higher forces are required to overcome the critical driving force for martensitic transformation. The obtained results showed that this effect is more dominant than the generated temperature suppressing the SIMT.

5. Conclusions

It was shown that dynamic tensile deformation significantly changes the mechanical properties of the thermomechanically processed 3Mn–Al and 5Mn–Al steels compared to static conditions. The following conclusions have been drawn:

The dynamic deformation increases both the strength and plastic properties as compared to the static tensile tests. The tensile strength increased by 300 and 260 MPa for the steels containing 3% and 5% Mn. A smaller increase in strength of 5Mn steel is due to its higher dislocation density before plastic deformation. In both steels, little increase in plasticity of 6% for 3Mn steel and 2% for 5Mn steel was recorded. Increasing the strain rate from 250 to $1000\,s^{-1}$ did not affect significantly the mechanical properties.

EBSD maps showing the distribution of grain boundaries in the microstructure indicated the dynamic recovery taking place during dynamic deformation in both steels. This is due to the temperature generation during deformation. The dominance of high-angle boundaries forming fine grains in case of 5Mn steel indicates a higher temperature increase during its deformation compared to the 3Mn steel, where the substructure with numerous low-angle boundaries was privileged.

According to the XRD and EBSD results, although the generated temperatures rose the SFE of the austenite, all fraction of this phase was transformed to strain-induced martensite during dynamic deformation. The amount of highly deformed martensite (≈14% and ≈7% in 3Mn and 5Mn steels, respectively) was similar to the RA before deformation. The applied tensile stresses favored the intense martensitic transformation.

Conflict of Interest

The authors declare no conflict of interest.

Data Availability Statement

The data that support the findings of this study are available from the corresponding author upon reasonable request.

[1] A. Mangipito, F. Lombardi, F. D. Sanvito, M. Pavicević, S. Quoilin, E. Colombo, *App. Energy.* **2022**, *312*, 118676.

[2] L. Nicoletti, A. Romano, A. Konig, F. Schockenhoff, M. Linkamp, *World Electric Veh. J.* **2022**, *11*, 63.

[3] P. Wang, *Vibroeng. Proc.* **2020**, *33*, 78.

[4] B. Hance, *SAE Inter. J. Mater. Manuf.* **2018**, *11*, 505.

[5] M. Y. Sherif, C. Garcia Mateo, T. Sourmail, H. K. D. H. Bhadeshia, *Mater. Sci. Technol.* **2004**, *20*, 319.

[6] W. Bleck, X. Guo, Y. Ma, *Steel Res. Int.* **2017**, *88*, 1700218.

[7] V. Alcantara, V. H. Pelaez, *J. Mech. Civil Eng.* **2022**, *19*, 37.

[8] A. Kwiatkowski da Silva, G. Inden, A. Kumar, D. Ponge, B. Gault, D. Raabe, *Acta Mater.* **2018**, *147*, 165.

[9] E. De Moor, D. K. Matlock, J. G. Speer, M. J. Merwin, *Scr. Mater.* **2011**, *64*, 185.

[10] A. Śmiglewicz, M. Jabłońska, W. Moćko, K. Kowalczyk, E. Hadasik, *Arch. Metall. Mater.* **2017**, *62*, 2255.

[11] S. J. Hiermaier, in *Structures Under Crash And Impact: Continuum Mechanics, Discretization And Experimental Characterization*, Springer, New York **2008**.

[12] Z. Gronostajski, A. Niechajowicz, R. Kuziak, J. Krawczyk, S. Polak, *J. Mater. Proc. Tech.* **2017**, *242*, 246.

[13] A. Kozlowska, A. Grajcar, A. Janik, K. Radwański, U. Krupp, K. Matus, M. Morawiec, *Arch. Civil Mech. Eng.* **2021**, *21*, 133.

[14] W. A. Poling, E. De Moor, J. G. Speer, K. O. Findley, *Metals* **2021**, *11*, 375.

[15] S. Sevsek, C. Haase, W. Bleck, *Metals* **2019**, *9*, 344.

[16] Z. He, H. Yang, Y. He, W. Zheng, Z. Guan, L. Li, *J. Mater. Res. Tech.* **2020**, *9*, 11611.

[17] H. Kim, J. Lee, F. Barlat, D. Kim, M. G. Lee, *Acta Mater.* **2015**, *95*, 435.

[18] M. Wang, M. X. Huang, *Acta Mater.* **2020**, *188*, 551.

[19] M. Nasim, B. C. Edwards, E. A. Wilson, *Mater. Sci. Eng. A* **2000**, *281*, 56.

[20] S. H. Song, R. G. Faulkner, P. E. J. Flewitt, *Mater. Sci. Eng. A*, **2000**, *281*, 23.

[21] A. Grajcar, D. Woźniak, A. Kozłowska, *Arch. Metall. Mater.* **2016**, *61*, 811.

[22] Sente software Ltd., A Collection of Free Downloadable Papers on The Development and Application of JMatPro, **2005**, http://www.sentesoftware.co.uk/biblio.html (accessed: february 2022).

[23] A. A. Alabi, Q. Wang, J. A. El-Awady, D. Raabe, M. Zaiser, *Nat. Commun.* **2021**, *12*, 1845.

[24] P. Landau, S. Osovski, A. Venkert, V. Gartnerova, D. Rittel, *Sci. Rep.* **2016**, *6*, 37226.

[25] J. Marcisz, J. Janiszewski, *Arch. Metall. Mater.* **2019**, *64*, 1151.

[26] S. Wright, M. Nowell, *Microsc. Microanalysis* **2006**, *12*, 72.

[27] A. A. Alabi, P. L. Moore, L. C. Wrobel, J. C. Campbell, W. He, *J. Constr. Steel Res.* **2018**, *150*, 107254.

[28] C. Yang, D. Li, T. Zhu, S. Xiao, *Adv. Mech. Eng.* **2016**, *8*, 1.

[29] H. Fan, Q. Wang, J. A. El-Awady, D. Raabe, M. Zaiser, *Nat. Commun.* **2021**, *12*, 1845.

[30] W. Wang, Y. Ma, M. Yang, P. Jiang, F. Yuan, X. Wu, *Metals* **2018**, *8*, 11.

[31] T. Chiyatan, V. Uthaisangsuk, *Mater. Sci. Eng. A* **2020**, *779*, 139125.

[32] J. V. Slycken, P. Verleysen, J. Degriecki, L. Samek, B. C. De Cooman, *Metall. Mater. Trans. A* **2006**, *37*, 1527.

[33] T. Rong, L. Lin, B. C. De Cooman, W. Xi-chen, S. Pang, *JISRI* **2006**, *13*, 51.

[34] M. B. Jabłońska, K. Jasiak, K. Kowalczyk, I. Bednarczyk, M. Skwarski, M. Tkocz, Z. Gronostajski, *Mater. Sci.* **2022**, *40*, 1.

[35] J. Talonen, H. Hanninen, P. Nenonen, G. Pape, *Metall. Mater. Trans. A* **2005**, *26*, 421.

[36] Z. S. Motlagn, A. Momeni, B. Tolaminejad, V. Javaheri, M. Soltanalinezhad, *Mater. Chem. Phys.* **2022**, *279*, 125771.